Reprinted from MONTHLY WEATHER REVIEW, Vol. 114, No. 3, March 1986
American Meteorological Society

The Geographical Distribution and Seasonality of Persistence in Monthly Mean Air Temperatures over the United States

H. M. VAN DEN DOOL AND W. H. KLEIN

J. E. WALSH

The Geographical Distribution and Seasonality of Persistence in Monthly Mean Air Temperatures over the United States

H. M. VAN DEN DOOL AND W. H. KLEIN

Department of Meteorology, University of Maryland, College Park, MD 20742

J. E. WALSH

Department of Atmospheric Science, University of Illinois, Urbana, IL 61801

(Manuscript received 15 June 1984, in final form 22 September 1985

ABSTRACT

Eighty years of monthly mean station temperatures are used to evaluate the persistence of monthly air temperature anomalies over the United States. The geographical and seasonal dependences of the monthly persistence are described in terms of the day-to-day persistence of temperature anomalies, the influence of the large-scale atmospheric circulation, and inferred associations with the slowly varying properties of the earth's surface.

The monthly persistence is generally smallest in the continental interior and largest in coastal regions. The seasonality of this spatial pattern is quite small, although the continental interior is characterized by a summer maximum. For the country as a whole, persistence is highest (0.30) in winter and summer and least (0.15) in fall and spring. For both raw and detrended data, the anomaly pattern correlations at lags of two and three months are much larger than would be expected from a first-order Markov process.

The pattern of persistences computed using day-to-day autocorrelations shows that the presence of nearby bodies of water increases the month-to-month persistence over that to be expected from daily weather fluctuations. This finding is consistent with the results derived from an intuitive energy balance model in which the soil (or ocean) surface layers and the atmospheric boundary layer respond to prescribed daily fluctuations in the free atmosphere.

Local surface influences are also implied by the fact that the 700-mb circulation-derived anomalies of monthly temperature have fewer spatial degrees of freedom than do the actual anomalies. While the large-scale circulation accounts for about half of the winter temperature persistence, small-scale effects, as well as the effects of the antecedent month's circulation, contribute substantially to the persistence of summer temperatures.

1. Introduction

This is a paper about persistence of anomalies in monthly mean air temperature (MMAT) near the earth's surface over the contiguous United States. Our goal is twofold. The first is to describe the geographical distribution and seasonality in month-to-month persistence of MMAT anomalies. The second is to understand why certain areas and certain seasons have higher persistence than others. An anomaly is defined here as a departure from a long term mean, and persistence is used here in a *statistical sense* that can be equated to month-to-month correlation at most places. We will not be dealing with specific cases of persistently anomalous weather conditions that occur *occasionally.*

Persistence of anomalies is an interesting phenomenon for many reasons. Thorough knowledge of persistence of various weather elements can be considered the basis for the lazy man's forecast. In fact, (damped) persistence of anomalies provides us with a reference skill level (over climatology) that has to be surpassed by credible operational forecasts. At the same time, the level of persistence for a given variable at a given site, season and height is interesting for its own sake. Persistence describes the typical time scale of departures from normal and therefore gives information about the dynamics of the atmosphere and the interaction of the atmosphere with the lower boundary, the ocean in particular.

Persistence of MMAT anomalies over the United States was extensively studied by Namias (1952, 1953), Dickson (1967) and van den Dool (1984). For slightly longer time scales (season, year) and for other areas, reference is made to Namias (1978), van den Dool and Nap (1981), Madden (1977), van Loon and Jenne (1975) and Klein (1985a). In the papers by Namias (1952) and Dickson (1967), the seasonality and spatial variability of MMAT anomaly persistence was described with data available at the time. In several of the above mentioned papers, the observation was made that persistence is higher in areas where the prevailing winds undergo an oceanic trajectory. Much of the present paper will explore why persistence is high near some of the oceans and small over most of the interior of the United States.

Describing the seasonality and spatial variability is not as easy as it may seem. Even though we will use 80 years of (probably) good quality monthly data at 61 stations, we may not be able to tell for sure whether

the correlation of MMAT anomalies from January to February at Kansas City differs significantly from zero, whether MMAT anomalies at Omaha in spring are more persistent than those in Washington or whether the seasonality in Dodge City is real or just a sampling fluctuation. We will limit the discussion to those findings which we think are likely to be reproducible in independent data. In order to suppress sampling fluctuations, we will generally use pooled data. That is to say, when we describe the geographical distribution of MMAT persistence, we will pool the data into a year-round data-mode, thereby purposely sacrificing the seasonality. Likewise, when discussing the seasonality, all data will be pooled into a country-wide data-mode, thereby purposely sacrificing the geographical variations. In addition to sampling fluctuations, we have to deal with problems such as trends. Trends, or very low frequency variability, could be of real interest here and may in fact explain month-to-month persistence. However, at many places trends are due to growth of the urban heat island, changes in exposure of the instrument, etc. (e.g., Cayan and Douglas, 1984). Somewhat over-conservatively, we will therefore detrend data by taking out a running 29-year mean. Frequently, we will discuss results based on both raw and detrended data.

Before exploring month-to-month persistence as such, it seems appropriate to ask whether it follows straightforwardly from day-to-day persistence. Therefore, we will derive (in section 4) from daily temperature statistics what level of month-to-month persistence can be expected at a given station. This will enable us to identify those areas where the actual month-to-month persistence is higher than expected from day-to-day weather fluctuations. This approach is complementary to Madden and Shea's (1978) search for potential predictability. They tried to find areas where the observed interannual variability in monthly means (of surface air temperature) is larger than can be expected from daily weather alone.

A central issue in this paper is whether persistence in MMAT anomalies could be a combination of the persistence caused by large-scale flow anomalies aloft, and the persistence due to interaction of the atmosphere with the earth's surface. If temperature in the planetary boundary layer were completely determined by the circulation aloft, then persistence (and interannual variance) of MMAT anomalies should be equal to the persistence (and interannual variance) of MMAT in the free atmosphere. But interaction with the lower boundary may modify the spectrum of near-surface air temperature, especially at low frequencies, so that even if the free atmospheric temperature has a white spectrum, the MMAT in the boundary layer may have positive autocorrelation (and a smaller interannual variation).

To investigate the relative roles of large-scale processes and the more local interactions, we will create a MMAT data set over the years 1947–79 which reflects the large-scale processes only. This will be achieved by specifying MMAT from concurrent monthly mean 700 mb height using multiple linear regression equations of the type described by Klein (1983, 1985b). Although this method is not perfect, it should to a first approximation tell us how persistent MMAT anomalies would be in the absence of interaction with the lower boundary. We implicitly assume here that the interaction of atmosphere and earth's surface has a negligible feedback on the 700 mb height fields, or that the feedback is restricted to the atmospheric boundary layer. This approach is similar to that of Walsh et al. (1985) who tried to isolate snow cover and soil moisture effects by studying the MMAT residuals not accounted for by concurrent 700-mb height anomalies.

Although the paper is mostly concerned with the one month lag correlation of MMAT anomalies, we will also describe the behavior of the correlation function at longer lags up to 24 months. This will bring out such interesting features as the large summer-to-summer lag correlations which are very sensitive to detrending of the data.

In section 2, we will describe the data sources and the various ways to measure persistence. A description of the geographical distribution and seasonality of MMAT persistence follows in section 3. In section 4 a brief description is given of persistence at lags up to two years. In section 5, we compare day-to-day and month-to-month persistence. A comparison with persistence of specified MMAT anomalies is made in section 6. With the help of simple intuitive models, an attempt is made (in section 7) to understand the geography and seasonality of persistence. Conclusions and summary are given in section 8.

2. Data and analysis

a. Data

In this paper we use the following three data sets:

1) Eighty years of monthly mean air temperatures (MMAT) at 61 stations distributed rather evenly over the United States covering the period 1900–79. This is an updated version of the data described in Walsh and Mostek (1980). A list of stations is given in Table 1. Missing or obviously erroneous data (<0.1%) were replaced by climatological mean values.

2) Thirty-three years (1947–79) of *specified* MMAT at the same 61 stations. A brief description and discussion of the specification process is given below.

3) Twenty-nine years of daily mean temperatures (average of maximum and minimum temperature) at 12 stations covering the period 1951–79. The 12 stations are a subset of the 61 listed in Table 1 and are underlined. A few gaps due to missing or obviously

TABLE 1. 61 stations in the United States for which monthly mean air temperatures for the period 1900–79 were used. At 12 stations (name underlined) we used daily temperature data for 1951–79 as well.

Eastport, Maine	Hatteras, N.C.	Abilene, Tex.
Blue Hill, Mass.	Asheville, N.C.	Galveston, Tex.
Albany, N.Y.	Charleston, S.C.	El Paso, Tex.
Oswego, N.Y.	Macon, Ga.	Havre, Mont.
Montreal, Quebec	Jacksonville, Fla.	Helena, Mont.
New York, N.Y.	Pensacola, Fla.	Sheridan, Wyo.
Washington, D.C.	Key West, Fla.	Denver, Colo.
Lynchburg, Va.	New Orleans, La.	Santa Fe, N. Mex.
Pittsburgh, Pa.	Vicksburg, Miss.	Boise, Idaho
Cincinnati, Ohio	Little Rock, Ark.	Salt Lake City, Utah
Columbus, Ohio	St. Louis, Mo.	Winnemucca, Nev.
Detroit, Mich.	Des Moines, Iowa	Phoenix, Ariz.
Alpena, Mich.	Bismarck, N. Dak.	Yuma, Ariz.
Marquette, Mich.	Rapid City, S. Dak.	Spokane, Wash.
Madison, Wis.	Huron, S. Dak.	Walla-Walla, Wash.
Duluth, Minn.	Omaha, Nebr.	Portland, Oreg.
Minneapolis, Minn.	North Platte, Nebr.	Mt. Shasta, Calif.
Chicago, Ill.	Topeka, Kans.	Sacramento, Calif.
Cairo, Ill.	Dodge City, Kans.	San Francisco, Calif.
Nashville, Tenn.	Amarillo, Tex.	Long Beach, Calif.
		San Diego, Calif.

erroneous observations were filled in by linear interpolation in time.

The calculations described below involve lagged products. In order to evaluate a lagged product involving December 1979, data of 1980 were used. In order to construct running means from daily data (data set 3 only), data of 1950 and 1980 were used.

The specification of MMAT at the 61 stations (the second data set) was done by constructing specification equations based on pointwise screening of monthly mean 700 mb heights. The resulting specification equations are of the form

$$\tilde{T}(s, m, j) = \sum_i \alpha_i(s, m)\hat{H}_i(m, j) \qquad (1)$$

where $\tilde{T}$ is the specified MMAT anomaly at station s in month m and year j, $\hat{H}$ is the observed 700 mb monthly mean height anomaly, i is a grid point index (i = 1, 91, running through the area 180°W, 50°W, 20°N and 80°N) and the α's are empirical coefficients determined by the screening process. The number of nonzero α_i's was determined by a 2% F-test criterion and ranges from two to seven. For further details about this methodology, the reader is referred to Klein (1983, 1985b) and Walsh (1984). Since 34 years of data are a small sample, we combined each month with its two neighboring months to triple the sample size. Thus equations for the month of February were derived from data for January, February and March, but applied to February only. For March, we used data for February, March and April and so on. In contrast to Klein (1983, 1985b), we purposely did not include the MMAT anomaly of the previous month as a predictor in the screening process. Therefore, our data set should reflect the synchronous averaged circulation to the extent that it affects the monthly mean surface air temperature. The specification approach has the drawback that we have only dependent data, so that the equations may have picked up some chance correlations and thus specified more variance in MMAT than they should; this may amount to 5 to 10% for four α_i's $\neq 0$ (Klein, 1983).

b. Analysis

Let $T(s, m, j)$ denote MMAT at station s (s = 1, 61), calendar month m (m = 1, 12) and year j (j = 1, 80). The mean over the years $j1$ to $j2$ is given by

$$\bar{T}(s, m) = \frac{1}{N}\sum_{j=j1}^{j2} T(s, m, j)$$

and the temporal standard deviation by

$$\mathrm{sdt}(s, m) = \left[\frac{1}{N}\sum_{j=j1}^{j2} [T(s, m, j) - \bar{T}(s, m)]^2\right]^{1/2}$$

where $N = j2 - j1 + 1$. Using the above, each $T(s, m, j)$ can be replaced by the standardized anomaly

$$\hat{T}(s, m, j) = \frac{T(s, m, j) - \bar{T}(s, m)}{\mathrm{sdt}(s, m)}.$$

We can now define the temporal correlation coefficient as

$$\mathrm{TC}(s, m, \tau) = \frac{1}{N}\sum_{j=j1}^{j2} \hat{T}(s, m, j)\hat{T}(s, m + \tau, j) \qquad (2)$$

where τ is the lag in units of months. The TC measures the degree of similarity of anomalies in MMAT at station in two months separated by τ as evidenced by records over many years of data.

Starting from $\hat{T}(s, m, j)$, we can further define a spatial average by

$$[\hat{T}(m, j)] = \frac{1}{61}\sum_{s=1}^{61} \hat{T}(s, m, j)$$

and a (spatial) standard deviation by

$$\mathrm{sds}(m, j) = \left\{\frac{1}{61}\sum_{s=1}^{61} [\hat{T}(s, m, j) - \hat{T}(m, j)]^2\right\}^{1/2}.$$

This leads to the definition of a pattern correlation coefficient:

$$\mathrm{PC}(m, \tau, j) = \frac{\frac{1}{61}\sum_{s=1}^{61} \{\hat{T}(s, m, j)\hat{T}(s, m + \tau, j) - [\hat{T}(m, j)][\hat{T}(m + \tau, j)]\}}{\mathrm{sds}(m, j)\,\mathrm{sds}(m + \tau, j)}. \qquad (3)$$

The PC measures the degree of similarity of MMAT standardized anomaly patterns over the coterminous United States appearing in year j in two months separated by τ.

Note the difference between TC and PC. TC is a function of the station (s), the basemonth (m) and the lag (τ) (and $j1$, $j2$), whereas PC is a function of the basemonth m, the lag τ and the year j (and implicitly $j1$ and $j2$). When studying the geographical distribution of month-to-month correlation, we will obviously use TC, while seasonality in month-to-month persistence on a continental scale can be studied conveniently with PC.

For a given basemonth m and lag τ, we can consider the entire distribution of PC (m, τ, j) for all years j. Apart from the climatological mean (PC), the standard deviation of the PC's around that mean is of interest. For an expected $\langle \mathrm{PC} \rangle = 0$ and a normal distribution, the standard deviation is governed by

$$\mathrm{sd_{PC}} = \frac{1}{(N_e - 2)^{1/2}}, \tag{4}$$

where N_e is the effective number of independent observations over the United States. Even though the above assumptions are not exactly satisfied, we will calculate N_e from estimates of $\mathrm{sd_{PC}}$ over 80 years of data. This yields some idea about the spatial scales of the MMAT anomaly pattern.

A disadvantage of (3) is that it considers anomalies relative to a continental average. As a result two months that are uniformly cold or warm over the entire United States are not considered persistent. To overcome this problem, we will also look at PC* defined by

$$\mathrm{PC}^*(m, \tau, j) = \frac{\frac{1}{61}\sum_{s=1}^{61} \hat{T}(s, m, j)\hat{T}(s, m+\tau, j)}{\mathrm{sds}^*(m, j)\,\mathrm{sds}^*(m+\tau, j)}, \tag{5}$$

in which continental averages are no longer subtracted from the standard deviation, i.e.,

$$\mathrm{sds}^*(m, j) = \left\{\frac{1}{61}\sum_{s=1}^{61} [\hat{T}(s, m, j)]^2\right\}^{1/2}.$$

Rather than looking at $\mathrm{PC}(m, \tau, j)$ for each year, we will be interested in the average PC over all years. Instead of averaging PC derived from (3), we can also redefine PC by summing through over all years:

$$\mathrm{PC}(m, \tau) = \frac{1}{M}\sum_{s=1}^{61}\sum_{j=j1}^{j2} \hat{T}(s, m, j)\hat{T}(s, m+\tau, j) \tag{3a}$$

where $M = 61N$. This has the advantage of vanishing $[\hat{T}(s, m, j)]$, $\mathrm{sds}(m, j) = 1$ and no ambiguity whether to use a PC or a PC*. On the other hand, (3a) does not allow us to estimate N_e from (4), so we will use it only where necessary.

Most of the results discussed below will be for detrended data. Detrending was achieved by removing a 29-year running mean. That is, $T(s, m, j)$ was replaced from the outset by

$$T(s, m, j) - \bar{T}(s, m, j)$$

where

$$\bar{T}(s, m, j) = \frac{1}{29}\sum_{k=j-14}^{j+14} T(s, m, k).$$

For $j \leqslant j1 + 14$ ($j \geqslant j2 - 14$) the summation is over $k = j1$ to $j1 + 28$ ($k = j2 - 28$ to $j2$). The purpose of detrending is to remove undesirable contributions to low frequency variability from changes in environment and observational location. But detrending is arbitrary and may take out physically interesting parts of the low frequency variability. Therefore, where appropriate, we will display results with and without detrending.

3. Description of spatial variation and seasonality

We calculated the temporal correlation TC (s, m, τ) for 61 stations, 12 basemonths, 3 lags (τ = 1, 2 and 3 months), 3 periods (1900–39, 1940–79 and 1900–79), raw data and detrended data. Since one of our major concerns is the reliability and reproducibility of the results, we have averaged TC over seasons and the whole year in the following symbolic way (for $\tau = 1$ only):

$$\text{Winter} = (\mathrm{N/D} + \mathrm{D/J} + \mathrm{J/F} + \mathrm{F/M})/4$$

$$\text{Spring} = (\mathrm{F/M} + \mathrm{M/A} + \mathrm{A/M} + \mathrm{M/J})/4$$

$$\text{Summer} = (\mathrm{M/J} + \mathrm{J/J} + \mathrm{J/A} + \mathrm{A/S})/4$$

$$\text{Fall} = (\mathrm{A/S} + \mathrm{S/O} + \mathrm{O/N} + \mathrm{N/D})/4$$

$$\text{Year} = (\mathrm{D/J} + \cdots \mathrm{N/D})/12.$$

(In spite of averaging over seasons and the year, we are studying month-to-month persistence!!)

As can be seen from Eq. (2), averaging over 4 or 12 months is identical to pooling 4 or 12 months together. The distribution of the yearly mean month-to-month correlation of MMAT anomalies for detrended data over 1900–79 is shown in Fig. 1. The number of pairs of data involved per station is $80 \times 12 = 960$. Assuming a normal distribution for TC and an expected value $\langle \mathrm{TC} \rangle = 0$, the sampling error of the quantity shown in Fig. 1 should be $1/\sqrt{958} = 0.03$. At all stations the autocorrelation in the yearly pooled data mode is clearly larger than zero. In the interior of the country, MMAT anomalies are short-lived (TC $\approx$ 0.1). However, at the West-, East- and Gulf coasts, the southwest desert and the Great Lakes area, TC is appreciably higher (up to 0.47 in San Diego).

Splitting the 1900–79 period into 1900–39 and 1940–79, we can check the stability of Fig. 1. Since the difference between the two periods (Fig. 2) rarely exceeds 0.13,[1] we accept the null hypothesis that the

[1] For forty years the sampling error in TC is $1/\sqrt{478} = 0.046$. Therefore the difference between two TC's based on 40 years of data has $0.046 \times \sqrt{2} = 0.065$ standard deviation.

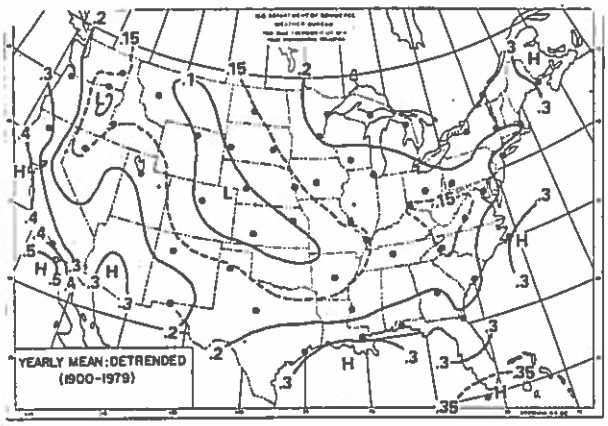

FIG. 1. The month-to-month correlation of monthly mean surface air temperature anomalies over the United States for the period 1900–79, on a yearly basis. The analysis is based on data at 61 stations located by the dots. The correlation is calculated according to Eq. (2).

month-to-month autocorrelations during the first and second 40-year periods were essentially the same. (The isolated very large difference at Mount Shasta, California is more likely associated with the relocation of the observational site in 1957 than with a physically interesting change in TC over the years.) In other words 40 years should be enough to establish the annual mean pattern of month-to-month correlation over the United States. It is therefore quite surprising that Dickson (1967) found a completely different pattern (his Fig. 1) with 60 or more years of data, a pattern that, moreover, was confirmed recently by Karl (1985). Both Karl and Dickson used statewide temperature as opposed to our station data. Since persistence is largely due to fairly local processes (as we shall see below) state averaged temperature is not a desirable parameter to study persistence.

Figure 1 is the most reliable description of the geography of TC variations that we can give with 80 years of data. Obviously, the geography may be seasonally dependent. Without denying that, it is fair to state that the sampling error in a map of TC for one pair of months over 80 years is about 0.11, so there is no point in presenting or explaining all the details in such maps. Instead, we show (Figs. 3–6) month-to-month persistence of MMAT-anomalies in a seasonally pooled data mode, for the period 1900–79. The sample size is $80 \times 4 = 320$, leading to about 0.06 sampling error at every station in any of these maps. Perhaps the most striking feature is that Figs. 3 to 6 are relatively similar, or that seasonality is small. The most notable exception is the appearance of an interior maximum (axis Texas to Wisconsin) in the summer season. Closer inspection reveals that the interior minimum is most widespread in fall and spring. Although the minimum east of the Rocky Mountains in winter is deep (some values negative), it is small in extent, and, towards the eastern portion of the continent, persistence in winter is actually quite high.

All of the above results (Figs. 1–6) were for detrended data. The effect of detrending is almost invariably a reduction of month-to-month correlation. That is to be expected since all frequencies < 1 cycle per 4 months contribute (by definition) positively to one-month lag autocorrelation. Obviously, detrending takes away mostly low frequencies, thereby decreasing autocorrelation. Without detrending, the large area with TC < 0.1 in Fig. 1 would have shrunk to just one city (Dodge City); at Key West TC would be 0.45 and at San Diego we would see TC = 0.63 instead of 0.47. Since the contribution of trends is largest in summer, we restrict ourselves here to discussing the trend contribution to TC in that season (Fig. 7). Because of the small scales, we avoided drawing isolines. As can be seen from Fig. 7, and from Cayan and Douglas (1984), the trend contributes little islands of 0.2 or more in many cities. Therefore we feel confident that detrending was the right thing to do in order to reduce effects associated with the growing urban heat island of several

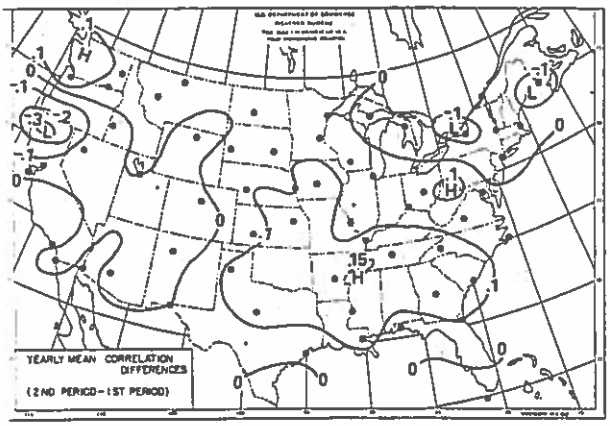

FIG. 2. The difference in month-to-month correlation, on a yearly basis, between 1900–39 and 1940–79.

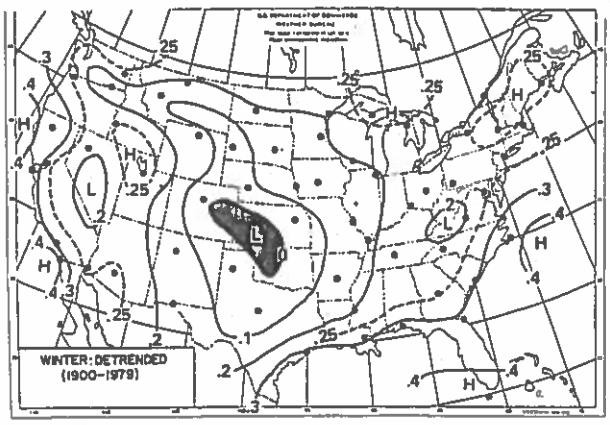

FIG. 3. As in Fig. 1 but for winter. Shading represents negative correlations.

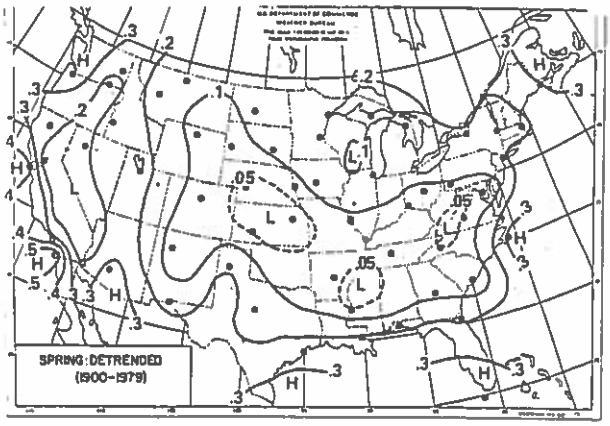

FIG. 4. As in Fig. 1 but for spring.

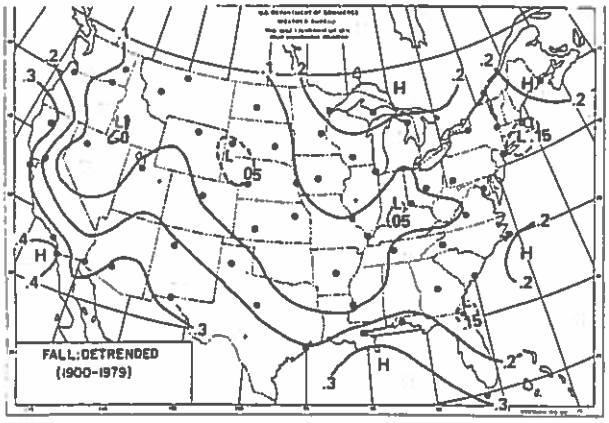

FIG. 6. As in Fig. 1 but for fall.

cities (Washington, San Diego, New Orleans . . .) or relocation of the observational site (Eastport, Maine in 1956). On the other hand, a large "trend" (≈0.05–0.10) also appears over several parts of the rural interior; here we may have filtered out some of the low-frequency variability that we intend to describe and explain. It is for this reason that in most of the graphs to follow, we display results for both *raw* and *detrended* data. Since the trend contribution is not particularly large along the axis of Texas to Wisconsin, there is no reason to believe that the summer maximum in those areas (see Fig. 5) is only due to suspect low frequency variability. Finally it should be pointed out that further detrending (15, 11, etc.—year running means) does not further reduce TC substantially.

Figures 3 to 6 already gave some impression of seasonality for all 61 stations. However, pooling all 61 cities together and employing the PC according to Eq. (3) gives the most condensed and reliable impression of seasonality. The pattern correlations, $PC(m, \tau, j)$ as well as $PC^*(m, \tau, j)$, were calculated for all years ($j = 1900, \cdots 1979$), 3 lags ($\tau = 1, 2, 3$ months) and all basemonths. At this point, we will discuss only

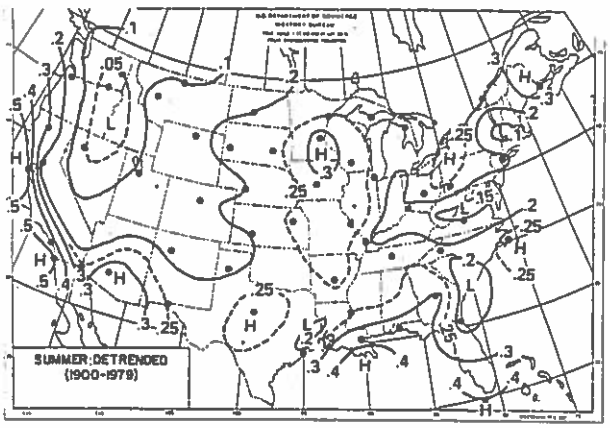

FIG. 5. As in Fig. 1 but for summer.

$$\overline{PC}(m, 1) = \sum_{j=1}^{80} PC(m, 1, j)/80.$$

Other forms of averaging such as using (3a) were tried out with results essentially similar to those described in this section. The average PC over 1900–79 for raw and detrended data as a function of the basemonth is shown in Fig. 8a. For both sets of data, there is a semiannual cycle in month-to-month correlation (with maxima in summer and winter) superimposed on a yearly mean ~0.2 correlation level. The effect of detrending is to decrease the autocorrelation in all months, but especially so in summer, thereby bringing out the much longer time scales that contribute to the persistence of MMAT anomalies in summer. More strict detrending (11-year mean out) does not further reduce the PC in summer, thereby indicating that the summer maximum also has some contributions from short time scales. This agrees with earlier results obtained with the TC (see Fig. 7). Using PC* instead of PC (see Fig. 8b) does make some difference, but the semiannual cycle in persistence continues to stand out. Comparison of PC and PC* shows that continental scale anomalies have positive (negative) persistence in summer (winter).

In Fig. 8c, we have plotted the spatial degrees of freedom (dof) as inferred from (4) using the standard deviation of PC around its mean over 1900–79. Our dof for MMAT anomaly fields seems to be about 10 for the entire United States, indicating the rather large spatial scale of such anomalies. Detrending decreases the dof, indicating that the spatial scale of the anomalies increases upon detrending the data stationwise. A likely explanation is that detrending takes away small-scale heat islands which apparently occur in all seasons. Since some of the assumptions underlying (4) may not be met, our dof estimate can only be a crude measure of the number of spatially independent cities. Nevertheless, we believe that 10 dof is a reasonable number and that the seasonality in dof is correct. In summer, the MMAT and circulation anomalies have typically

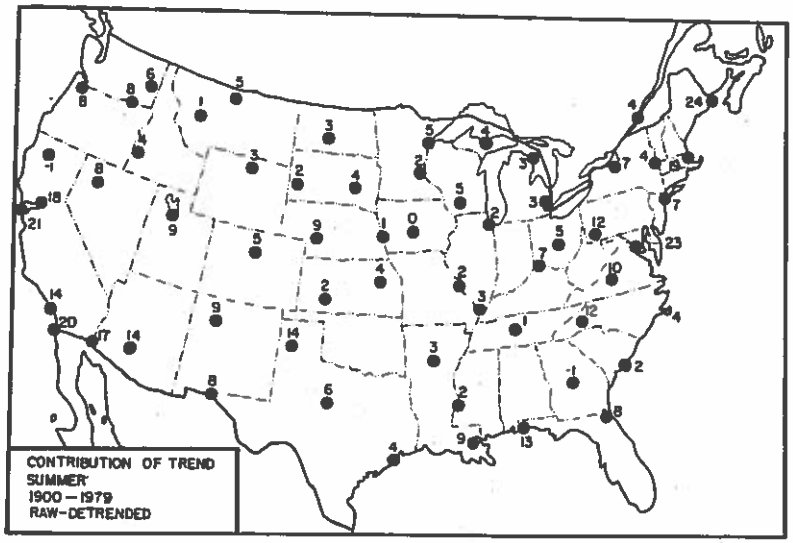

FIG. 7. Contribution of the trend (running 29-year mean) to persistence of monthly mean air temperature anomalies in summer over the United States during 1900–79. Values are multiplied by 100.

smaller spatial scale; therefore it seems reasonable that the dof in summer is larger.[2] Taking dof = 10 as an accurate estimate, we can estimate the sampling error in the PCs to be about $0.035 = 1/[(10 \times 80) - 2]^{1/2}$. Therefore, the difference between the persistence maxima ($\approx$0.30 in summer and winter) and the minima ($\approx$0.15 in fall and spring) is probably real and quite unlikely to be due to sampling errors. This is born out by considering average PCs over 1900–39 and 1940–79 separately (not shown). In both periods, the two-peak-two-valley structure, seen in Fig. 8, is present. Namias (1952) and Dickson (1967) found a similar distribution of persistence throughout the year.

4. Lags longer than one month

In this short section, we will describe the correlation of MMAT anomalies at lags of 1 to 24 months. In all other sections, we are essentially dealing with just the one month lag correlation. That would suffice if $\overline{PC}(m, \tau)$ could be related to $PC(m, 1)$ for all τ, and similarly for TC. The common assumption of a first order Markov process (for example) can be verified here. In order to keep the description concise, we will only show results pertaining to the pattern correlation PC according to (3).

Figure 9 shows iso-correlation lines in a month (vertical) vs lag (horizontal) plot. The month plotted along the vertical axis is the base month; that is, starting from January on the left, one will find along a horizontal

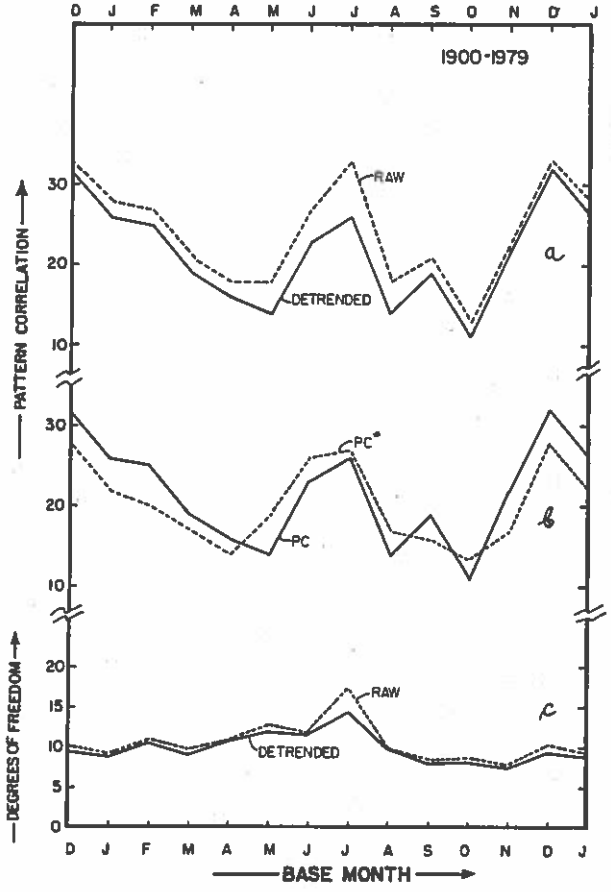

FIG. 8. Pattern correlation (%) of standardized MMAT anomaly patterns over the United States at lag 1 month as a function of the leading month. The years are 1900–79. In (a) we compare raw and detrended data, in (b) we compare PC excluding and PC* including continental scale anomalies (both detrended) and in (c) we give the spatial degrees of freedom associated with raw and detrended MMAT data, evaluated according to Eq. (4).

[2] Another test of (4) is to use monthly rainfall sums at the same 61 stations. Now we find dof to vary from 25 in winter to more than 60 in summer. This, again, seems quite reasonable. In summer, the dof is about equal to the number of stations (61), emphasizing the well-known spottiness of rainfall patterns in summer.

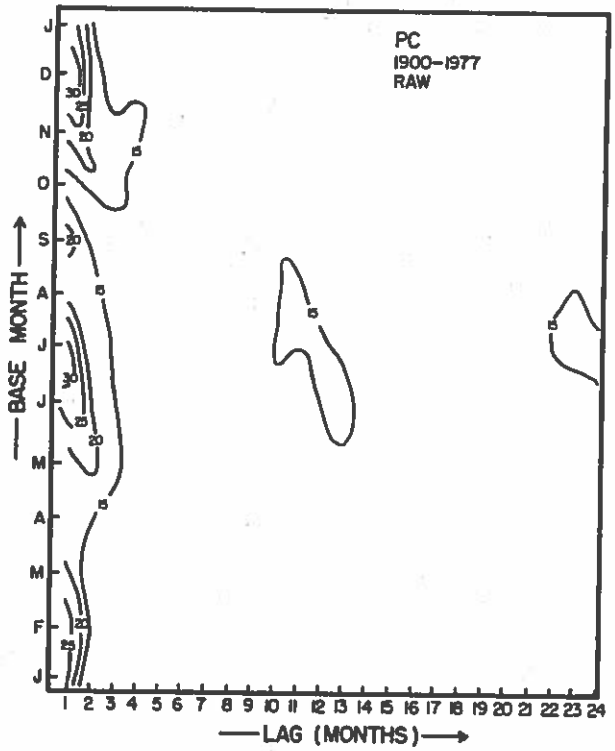

FIG. 9. Pattern correlation (%) of standardized MMAT anomaly patterns over the United States at lags from one month to two years as a function of season. Values less than 15% were not analyzed. The years are 1900–77 and data were not detrended.

line the average PC between January and February (lag 1), January and March (lag 2), January and April (lag 3), etc., up to 24 months. The years are 1900–77, and the data are *not* detrended. A vertical cross section along lag 1 month gives approximately the same values as plotted in Fig. 8a (curve labeled raw). Only values in excess of 0.15 are contoured. As expected, the PC decreases with increasing lag for $1 < \tau < 6$ months. But the summer months show larger than 0.15 correlation with summertime anomalies as much as one and two years later. The summer-to-summer persistence for seasonal means has been noted by several previous authors (Madden, 1977; Namias, 1978). The long time scale of MMAT anomalies is also visible in the slow decay of PC with increasing lag in summer for $1 < \tau < 4$ months. In contrast, the persistence maximum in January disappears rapidly with increasing lag. These observations reinforce our earlier conclusion that the persistence in summer is largely due to very low frequency variability on the scale of years, whereas in winter the anomalies have time scales of months.

A rather interesting feature of Fig. 9 is the inclination of the isolines towards the lower right. This tendency is so strong that at a lag of four months the maxima are occurring at basemonths May and November. In fact, with May as base month the PC increases from lag 1 to lag 2 months. Thus, deviations from a first order linear Markov process are large, mostly due to seasonality in PC. But even in yearly pooled data mode, the decay from lag 1 to 3 does not look like a first order process. The yearly mean PC over 1900–77 is 0.23, 0.15 and 0.12 for lag 1, 2 and 3, respectively. After detrending, these numbers are 0.20, 0.12 and 0.09. Thus for both raw and detrended data, the PC at lags 2 and 3 months remains very much larger than can be expected from a first order Markov process.

Finally, we should mention that the correlations at lag 1 and 2 years starting from summer MMAT-anomaly patterns change considerably upon detrending the data. The extent of the two maxima in basemonth–lag space (Fig. 9) is greatly reduced after removing the 29 year running mean, and the peak values are reduced to about 0.11. This once more emphasizes the multi-year time scale contributing to persistence in summer.

5. Day-to-day and month-to-month correlation

A natural question is whether month-to-month correlation of MMAT can be explained from day-to-day correlation alone. More precisely, if we calculate from a given data set the one day lag autocorrelation for daily data ($\rho_1(1)$) and if we *assume* that the autocorrelation of daily data at lag k days ($\rho_1(k)$) is given by

$$\rho_1(k) = [\rho_1(1)]^k, \tag{6}$$

i.e., the linear first order Markov assumption, then we can *expect* l day means to be correlated by

$$\rho_l^e(l) = \frac{\rho_1(1)\{1 - [\rho_1(1)]^l\}^2}{l[1 - \rho_1(1)^2] - 2\rho_1(1)[1 - \rho_1(1)^l]} \tag{7}$$

where $\rho_l(k)$ denotes the autocorrelation of l-day averages at a lag of k days. Equation (7) was derived for a discrete Markov process, but numerically it is virtually the same as an expression derived by Munk (1960) for continuous Markov processes. If $\rho_{30}^e(30)$ (e for expected) is the same as $\rho_{30}^c(30)$ (calculated or observed) then, indeed, month-to-month persistence can be understood from day-to-day persistence. In that case, there is no point to a physical explanation of month-to-month persistence, as such, since it follows from the chain of correlated daily values. To the extent that $\rho_{30}^e(30)$ differs from $\rho_{30}^c(30)$, daily data are not obeying a first order linear Markov process. To that end, studying $\rho_{30}^c(30)$ could be a lot more efficient than studying $\rho_1^c(k)$ for all $k \leq 30$ days. Departures from the linear first order Markov chain were studied by considering $\rho_1^c(k)$ for 500 mb heights by Gutzler and Mo (1983), Horel (1985), Trenberth (1985) and Roads and Barnett (1984) and for surface air temperature by Strauss and Halem (1981).

For 12 of the 61 stations we have daily data over 1951–80 at our disposal. We calculated temporal correlations in the following way. At each day (i) of the year (j), the input temperature data at station s were replaced by standardized anomalies; the mean and standard deviation were determined from the 30 data

points (1951–79) for just that calendar date. We then pooled the data of a given station in a year-round mode to calculate

$$\mathrm{TC}(s, \tau) = \frac{1}{N} \sum_{j=1}^{30} \sum_{i=1}^{365} \hat{T}(s, i, j)\hat{T}(s, i + \tau, j) \qquad (8)$$

where $N = 30 \times 365$. For $\tau = 1$ day, $\mathrm{TC}(s, \tau)$ gives us $\rho_1^c(1)$. The one-day lag autocorrelation, $\rho_1^c(1)$, thus calculated, ignores seasonality and, as we will see below, that is not a bad assumption. Values of $\rho_1^c(1)$ can be calculated from (8) for each month by summing over the days (j) of that month only. Upon applying a moving 5-, 15-, and 29-day mean average to the $\hat{T}(s, i, j)$ values and recalculating TC by (8), $\rho_5^c(5)$, $\rho_{15}^c(15)$ and $\rho_{29}^c(29)$ can easily be generated. Where necessary, data for December, 1950 and January, 1980 were used to construct the moving averages or evaluate lagged products in (8).

From the calculated first order autocorrelation, $\rho_1^c(1)$, we derived $\rho_5^c(5)$, $\rho_{15}^c(15)$ and $\rho_{29}^c(29)$ by employing (7). The results are presented in Table 2. The stations are listed in increasing order of $\rho_1^c(1)$; that is, from Albany (0.65) to San Diego (0.75). It is interesting that $\rho_1^c(1)$ is similar for these vastly different climates and seems to hover around 0.70. Based on $\rho_1^c(1) \approx 0.70$ month-to-month autocorrelation, $\rho_{29}^e(29)$ should be around only 0.05. At all stations $\rho_{29}^c(29)$ is larger than $\rho_{29}^e(29)$, the difference ranging from 0.04 at Denver to 0.25 and 0.30 at Portland and San Diego. It is obvious that the geographical variation in $\rho_{29}^c(29)$ is not the result of geographical variation in $\rho_1^c(1)$. Except for El Paso, the presence of nearby bodies of water seems to determine whether month-to-month persistence is larger than can be expected from day-to-day weather alone. We conclude here that the departure from a first order Markov process for surface air temperature is large at many stations. This is somewhat different from results arrived at with 500 mb heights where no significant departures from red noise were reported (Roads and Barnett, 1984)

New Orleans has a pronounced seasonality in month-to-month persistence of MMAT-anomalies similar to that for the country as a whole (shown in Fig. 8). In Fig. 10 the first order day-to-day correlation ($\rho_1^c(1)$) is plotted as a function of the calendar month, along with plots for $\rho_{29}^c(29)$ and $\rho_{29}^e(29)$. Not only is $\rho_1^c(1)$ too low to explain the overall level of $\rho_{29}^c(29)$, but also $\rho_1^c(1)$ does not even give a hint of the seasonality to be explained in $\rho_{29}^c(29)$. The lack of seasonality in $\rho_1^c(1)$ is not unique to New Orleans. At most of the 12 cities $\rho_1^c(1)$ is fairly constant throughout the year. The absence of a well-defined seasonality is a justification for compiling data in a year-round mode, as was done in Table 2.

It seems fair to consider $\Delta = \rho_{29}^c(29) - \rho_{29}^e(29)$ as a measure of potential predictability. After all, $\rho_{29}^e(29)$ is the amount of persistence in monthly mean anomalies to be expected due to just short-time-scale weather. Our approach is very similar to Madden and Shea (1978) who tried to calculate interannual variability of monthly means due to weather alone: the so-called climate noise or natural variability. In terms of indicating the cities with highest potential predictability, the present study largely agrees with Madden and Shea. However, using autocorrelation has the advantage that one immediately knows how to effectuate the potential predictability, thereby turning it into skill of forecasts.

Table 2 also gives calculated and estimated values of $\rho_5(5)$ and $\rho_{15}(15)$. For 5-day averages, the decay of autocorrelation at all cities is quite close to what can be expected from daily data. Actually, at some cities (Cincinnati), the decay is more rapid than expected for a first order Markov chain. This feature was reported also by Strauss and Halem (1981). At 15 days, the excess of spectral energy at low frequencies over a red noise spectrum becomes visible in all cities; $\rho_{15}(15)$ behaves similarly to $\rho_{29}(29)$.

TABLE 2. Yearly mean autocorrelation (%) of surface air temperature anomalies in 12 cities in the United States for the years 1951–79; $\rho_l(l)$ denotes the autocorrelation of averages over l days (l = 1, 5, 15 and 29) at a lag of l days (l = 1, 5, 15 and 29), i.e. $\rho_1(1)$, $\rho_5(5)$, $\rho_{15}(15)$ and $\rho_{29}(29)$ are considered. The column "E" refers to autocorrelation of time means to be expected because of the correlation of daily values, assuming a first-order Markov process. Column "C" is calculated from observed data, and C − E is the difference between calculated and expected.

		$\rho_{29}(29)$			$\rho_5(5)$			$\rho_{15}(15)$		
City	$\rho_1(1)$	C	E	C − E	C	E	C − E	C	E	C − E
Albany, N.Y.	65	14	4	10	26	29	−3	15	9	6
Denver, Colo.	66	8	4	4	30	30	0	16	9	7
Bismarck, N. Dak.	67	17	4	13	36	31	5	27	9	18
Dodge City, Kans.	67	11	5	6	34	31	3	21	10	11
El Paso, Tex.	70	27	5	22	36	35	1	30	11	19
Minneapolis, Minn.	70	19	5	14	33	35	−2	22	11	11
New Orleans, La.	70	26	5	21	37	35	2	30	11	19
Omaha, Nebr.	70	12	5	7	34	35	−1	19	11	8
Pittsburgh, Pa.	70	17	5	12	28	35	−7	19	11	8
Cincinnati, Ohio	71	16	6	10	28	37	−9	17	12	5
Portland, Oreg.	72	31	6	10	28	37	−9	17	12	5
San Diego, Calif.	75	37	7	30	48	42	6	42	15	27

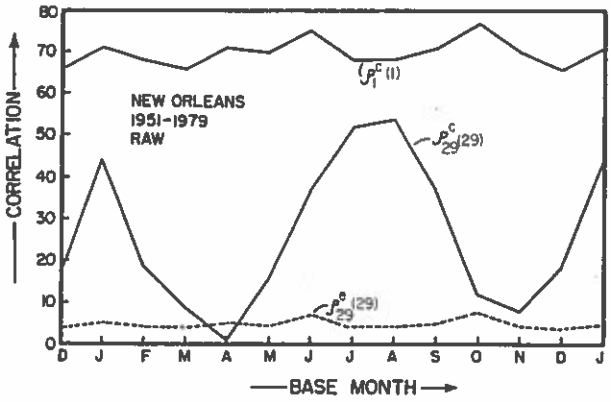

FIG. 10. Day-to-day and month-to-month autocorrelation (%) of temperature at New Orleans as a function of season. Here $\rho_k^c(k)$ denotes a (calculated) autocorrelation of averages over k days at a lag of k days. $\rho_{29}^c(29)$ is the month-to-month correlation to be expected on the basis of day-to-day correlation.

The entire procedure was repeated with detrended daily temperature data. Since we have only 30 years of data, taking out a running 29 years mean (as we did before) is meaningless. Instead, an 11 day–11 year running mean was subtracted to eliminate the annual cycle and multiyear trends in a smooth way. This treatment of the input data did not change our results significantly. In other words, the geographical distribution of $\rho_1^c(1)$ (no matter how calculated) does not explain [via (7)] the geographical distribution of $\rho_{29}^c(29)$.

6. Circulation-derived anomalies

Since weather near the surface can largely be explained from upper air charts, it seems reasonable to try to explain persistence in MMAT anomalies from persistence in concurrent anomalies in the free atmospheric flow. As was described in van den Dool and Livezey (1984), anomalies in monthly mean 700 mb heights over the United States exhibit a month-to-month autocorrelation that varies from 0.05 over the West Coast to 0.3 over the Southeast. This seems somewhat low to explain the much higher persistence of near-surface MMAT anomalies, especially along the West Coast. However, as shown in Klein (1983) and Klein (1985b), the optimum specification of MMAT for a United States city may involve grid points in the subtropics where 700 mb height anomalies tend to be quite persistent (Namias, 1959; van den Dool and Livezey, 1984; Walsh, 1984). For this reason, we constructed (see section 2) a data set of specified MMAT anomalies for all 61 stations based on monthly mean 700 mb height data over a large area observed during 1947–79. This data set reflects the 700 mb characteristics to the extent that the upper air flow is relevant to surface temperatures.

In the upper panel of Fig. 11 we show the average PC, according to Eq. (3), over the years 1947–79 for both the observed and specified MMAT data sets. The treatment for the two sets was exactly the same. The trend was over-conservatively removed by subtracting an 11-year running mean. As can be seen from Fig. 11, the PC, based on observed MMAT, is far higher than that based on specified data in most months. In summer, the specified data are particularly deficient in explaining the observed level of persistence of MMAT-anomalies. In the lower panel of Fig. 11, we further plotted the estimate of dof associated with either data set. The most interesting aspect is that specified MMAT-anomalies have fewer dof (that is larger spatial scale) than observed MMAT-anomalies. Thus, Fig. 11 leaves us with the impression that on top of circulation-explained anomalies, fairly small scale MMAT anomalies are of vital importance in explaining the observed level of persistence, especially in summer.

The results in Fig. 11 could actually be somewhat misleading because even if the two PC curves were identical, one cannot conclude that the large-scale circulation fully explains persistence in MMAT-anomalies. This is because the variance of the specified MMAT-anomalies is only 40–65% of the variance of observed MMAT. This problem can be overcome by splitting the observed MMAT standardized anomaly $[\hat{T}(s, m, j)]$ explicitly into two contributions:

$$\hat{T}(s, m, j) = \hat{T}_c(s, m, j) + \hat{T}_r(s, m, j) \qquad (9)$$

where the indices c and r refer to circulation explained and a residue. $\hat{T}_c$ reflects the large-scale upper air flow and $\hat{T}_r$ anything else, but we think of $\hat{T}_r$ as representing

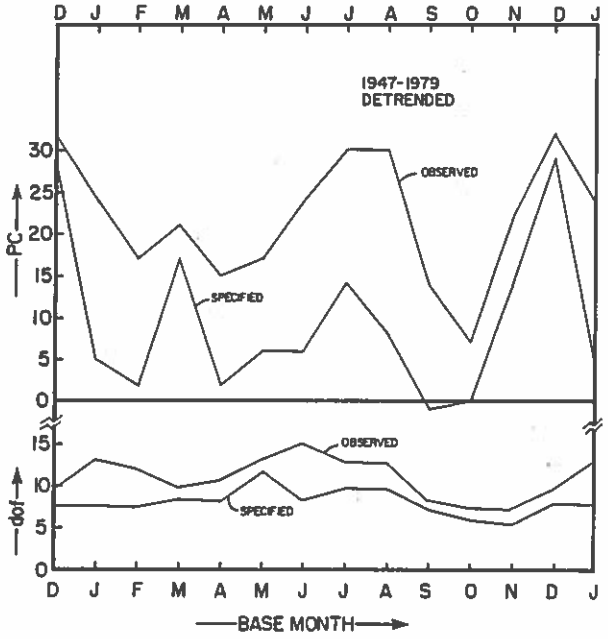

FIG. 11. Pattern correlation (%) of observed and specified standardized MMAT anomaly patterns over the United States as a function of season for the years 1947–79. Detrending was done by taking out a running 11-year mean. In the lower panel, the spatial degrees of freedom associated with observed and specified MMAT patterns are depicted.

mostly local processes. Note that $\hat{T}_c$ and $\hat{T}_r$ were both standardized by the standard deviation of the MMAT series over 1947–79 (appropriate for the month and station). This enables us to rewrite the definition of TC (Eq. (2)) as

$$\mathrm{TC}(s, m, \tau) = \frac{1}{N}\Big[\sum_j \hat{T}_r(s, m, j)\hat{T}_r(s, m+\tau, j) + \sum_j \hat{T}_c(s, m, j)\hat{T}_c(s, m+\tau, j) + \sum_j \hat{T}_r(s, m, j)\hat{T}_c(s, m+\tau, j) + \sum_j \hat{T}_c(s, m, j)\hat{T}_r(s, m+\tau, j)\Big], \quad (10)$$

and to rewrite the definition of PC [Eq. (3a)] as

$$\mathrm{PC}(m, \tau) = \frac{1}{M}\Big[\sum_s \sum_j \hat{T}_r(s, m, j)\hat{T}_r(s, m+\tau, j) + \sum_s \sum_j \hat{T}_c(s, m, j)\hat{T}_c(s, m+\tau, j) + \sum_s \sum_j \hat{T}_r(s, m, j)\hat{T}_c(s, m+\tau, j) + \sum_s \sum_j \hat{T}_c(s, m, j)\hat{T}_r(s, m+\tau, j)\Big] \quad (11)$$

where $M = 61 \times 33$. Equation (11) is identical to (10) except for the summing over all 61 cities. None of the terms on the right-hand side of (10) and (11) is a correlation in itself, but nevertheless the interpretation is straightforward. The lagged products $\hat{T}_c\hat{T}_c$ and $\hat{T}_r\hat{T}_r$, respectively, represent persistence of MMAT-anomalies associated with circulation aloft ($\hat{T}_c\hat{T}_c$) and persistence of MMAT-anomalies not accounted for by the large-scale circulation ($\hat{T}_r\hat{T}_r$). The $\hat{T}_r\hat{T}_r$ term would be large if, for example, the ocean created autonomously long-lived sea surface temperature (SST) anomalies which in turn forced MMAT-anomalies near the surface without altering the atmospheric flow aloft. The lagged cross-product $\hat{T}_r\hat{T}_c$ represents the influence of the present month's $\hat{T}_r$ on future 700 mb heights; in a sense, this is the feedback of MMAT-anomalies (created by processes other than the current large-scale flow) on the 700 mb height. Finally, the $\hat{T}_c\hat{T}_r$ term represents a spill-over effect of MMAT-anomalies into the next month. This term would be large if, for example, an SST anomaly created by large-scale atmospheric anomalies in month 0 feeds back on $\hat{T}_r$ in month +1 while the atmospheric circulation supporting the original $\hat{T}_c$ anomaly no longer exists.

Figure 12 shows the decomposition of PC into the four contributions evaluated according to (11). Because we used a slightly different definition of PC [(3a) in Fig. 12 versus (3) in Fig. 11], the PC curves in Figs. 11 and 12 are slightly different. In order to obtain smooth results, a 1-1-1 filter was applied before plotting Fig. 12. (This is in our case identical to pooling three months of data.) As was anticipated from Fig. 11, the $\hat{T}_c\hat{T}_c$ term alone is insufficient to explain the observed level of persistence. The winter maximum in persistence ($\approx$0.22) is due mainly to contribution of $\hat{T}_c\hat{T}_c$ and $\hat{T}_c\hat{T}_r$. Both of these terms peak in winter and have only weak summer maxima. Throughout most of the year, the $\hat{T}_c\hat{T}_r$ is larger than $\hat{T}_c\hat{T}_c$. The summer maximum in persistence ($\approx$0.24) contains contributions of all four terms, so it is not possible to single out one particular cause of persistence in summer. The largest of the four terms in summer is the $\hat{T}_r\hat{T}_r$ term. Even the feedback term in summer ($\hat{T}_r\hat{T}_c$) is larger than zero; this may be taken as weak, empirical, although not statistically significant, evidence for Namias' hypothesis about drought (Namias, 1980). It is also possible that specification equations, taking just 700 mb heights as specifiers, are not good enough to split an observed anomaly into $\hat{T}_c$ and $\hat{T}_r$. This may be the case in summer when less than 50% of the variance is captured by the specification equations (Klein, 1985b).

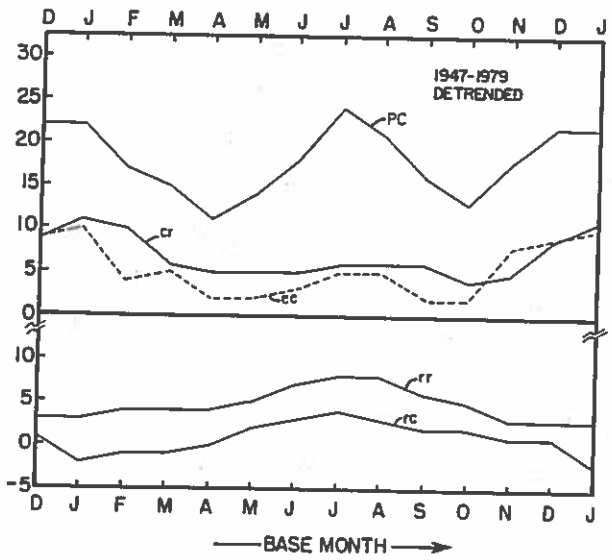

FIG. 12. The decomposition of the pattern correlation (in %; curve labelled PC) of observed standardized MMAT-anomaly patterns over the United States during 1947–79 into four contributions according to (11) as a function of season. The cc, rr, cr and rc terms represent lagged products of circulation specified and residual MMAT anomalies. A 1-1-1 smoother was applied on the cr, cc, rr and rc curves.

We have similarly decomposed the yearly mean TC at all 61 stations, using (10). Since the yearly mean TC is a small quantity, subject to considerable sampling fluctuations, a decomposition into four contributions has to be considered with caution. Rather than showing four maps, we have ordered the 61 cities according to decreasing yearly mean TC. Table 3 (upper part) shows the decomposition for those stations satisfying TC $>$ 0.25 (eight). With the exception of Macon, all of these stations are situated near large water bodies. Persistence of circulation-specified MMAT-anomalies explains only about 20% of the persistence level observed

TABLE 3. The yearly mean month-to-month correlation (%) of monthly mean air temperature at some cities in the United States. The period is 1947–79, and the data were detrended by removing an 11-year running mean. The yearly mean TC evaluated according to (2) is given in the first column. Columns 2 to 5, labeled *rr*, *cc*, *rc* and *cr* are the decomposition of TC according to (10), outlined in the text. The upper (lower) portion gives results for those eight cities where monthly temperature anomalies are most (least) persistent. The averages over these eight cities are included in the rows labeled mean. As a separate row, we have also listed results for Sacramento to highlight differences with San Francisco.

City	TC	*rr*	*cc*	*rc*	*cr*
San Diego, Calif.	40	18	8	1	12
San Francisco, Calif.	37	23	5	2	8
Long Beach, Calif.	35	20	4	2	9
Macon, Ga.	29	12	6	3	8
Portland, Oreg.	27	6	7	5	9
Pensacola, Fla.	26	9	6	4	6
New Orleans, La.	26	10	7	4	5
Galveston, Tex.	26	8	5	3	11
mean 8 highest	30.6	13.3	6.0	3.0	8.5
(Sacramento, Calif.	21	9	1	3	8)
Albany, N.Y.	9	−2	3	1	7
Helena, Mont.	9	3	1	0	6
Havre, Mont.	9	3	4	−4	6
Lynchburg, Va.	8	−1	5	2	3
Winnemuca, Nev.	8	4	4	−3	3
Rapid City, S. Dak.	8	2	2	−1	5
Sheridan, Wyo.	7	0	2	−1	7
Denver, Colo.	6	4	2	−1	1
mean 8 lowest	8.0	1.6	2.9	−0.9	4.8

at these cities. The largest contribution, in fact, comes from persistence in $\hat{T}_r$, especially at California's coast. In addition, a very substantial contribution (~28%) comes from the $\hat{T}_c\hat{T}_r$. In other words, the effects of atmospheric circulation continue to be felt even though the circulation itself no longer supports the MMAT-anomaly created in the previous month. Finally, the $\hat{T}_r\hat{T}_c$ term is the smallest of all, indicating that feedback of $\hat{T}_r$ on future 700-mb height anomalies is small.

The dramatic decrease of MMAT-anomaly persistence when traveling landward from California's coast (see Fig. 1) can best be analyzed by comparing the decomposition of TC for San Francisco (downtown station close to the coast) and Sacramento (only about 50 km to the east). The decrease from 0.37 in San Francisco to 0.21 in Sacramento can be ascribed fully to the decrease of the $\hat{T}_r\hat{T}_r$ term over this short distance. This is evidence that SST anomalies produce a large enhancement of MMAT-anomaly persistence right at the California coast line. Furthermore, the effects of such SST anomalies are confined to a zone of less than 50 km over which advection apparently can transport air that carries the SST-anomaly signature. This agrees with results of van den Dool and Nap (1981) for the Netherlands and Klein (1985a) for Canada and Alaska. Comparing the stations at the Gulf Coast with those in California we see that at the former stations $\hat{T}_r\hat{T}_r$ is much smaller. This indicates that, in contrast to the offshore waters of California, the Gulf of Mexico does not exhibit long lived SST-anomalies or the prevailing wind is directed less strongly onshore. Along the Atlantic coast, the $\hat{T}_r\hat{T}_r$ is even smaller (zero at Cape Hatteras), so the California current area seems to be the exception rather than the rule in thermally forcing the atmospheric boundary layer.

When going down the list of stations to very small annual mean TC, the decomposition becomes quite different. In the lower portion of Table 3 we have listed those eight stations satisfying TC < 0.10. All of these stations are away from the coastline, and most of them are well within the interior of the country. The bulk of the small persistence observed in these areas comes from the $\hat{T}_c\hat{T}_r$ term, while a small but positive contribution by $\hat{T}_c\hat{T}_c$ explains the remainder.

Summarizing (11) over all 12 months, we arrive at year-round country-wide figures. The month-to-month persistence in this most condensed format is due to $\hat{T}_c\hat{T}_r$ (36%), $\hat{T}_r\hat{T}_r$ (30%), $\hat{T}_c\hat{T}_c$ (27%) and $\hat{T}_r\hat{T}_c$ (6%) respectively. At lags 2 and 3 months, the $\hat{T}_r\hat{T}_r$ term becomes by far the most important of all, emphasizing either long-lived anomalies in surface properties or problems with the data sets due to relocation of the thermometer, city effects, etc.

7. Intuitive model

To a large extent, an instantaneous air temperature anomaly near the surface is caused by synchroneous large scale atmospheric circulation anomalies. However, interaction with the lower boundary may enhance the level of persistence of that anomaly far beyond that expected from the circulation alone. In this section we survey a few possible ways in which interaction with the lower boundary changes the autocorrelation and variance of air temperature anomalies. We will do this in the framework of a simple set of two energy balance equations given by

$$C_a \frac{d\hat{T}_a}{dt} = -\alpha(\hat{T}_a - \hat{T}_f) - \beta(\hat{T}_a - \hat{T}_s), \qquad (12)$$

$$C_s \frac{d\hat{T}_s}{dt} = \beta(\hat{T}_a - \hat{T}_s), \qquad (13)$$

where $\hat{T}_a$ and $\hat{T}_s$ are *instantaneous* anomalies in air and surface temperature, respectively; C_a and C_s are thermal inertias of the layer of air and the layer of soil, respectively, for which $\hat{T}_a$ and $\hat{T}_s$ are representative; α and β are heat transfer coefficients, respectively; and $\hat{T}_f$ is a prescribed time-varying free atmospheric temperature anomaly. The term $\alpha\hat{T}_f$ is the forcing of (12) and (13). It is easy to generate series of $\hat{T}_f$ with known autocorrelation and variance and to calculate autocorrelation and variance of $\hat{T}_a$ as a function of the interaction with the lower boundary. In particular, we are interested to see how the month-to-month correlation changes.

Using a random generator, 30 000 numbers (ϵ_i) were drawn from a normal distribution with zero mean and variance of one. Assuming an autocorrelation of 0.61 at lag 1 day, $\hat{T}_f$ values (sampled at 1.2 h interval) were generated by

$$\hat{T}_f(i+1) = (0.61)^{1/20}\hat{T}_f(i) + \epsilon_i.$$

The resulting $\hat{T}_f$ series was used to force a discretized version of (12) and (13) in which $\hat{T}_a$ and $\hat{T}_s$ are integrated forward in time with a time step of 1.2 hours (small enough for numerical stability). (We have chosen here a 0.61 lag 1 day autocorrelation for $\hat{T}_f$ because this leads, as we shall see below, to a lag 1 day autocorrelation for $\hat{T}_a$ of about 0.7 which is realistic over much of the United States.) In order to eliminate the effects of the spinup, we discarded the first 500 $\hat{T}_a$ and $\hat{T}_s$ values. The remaining 29,500 $\hat{T}_a$ and $\hat{T}_s$ were sampled at a one day interval (leaving 1475 values) and 30 day running means were constructed.

We will discuss the influence of the lower boundary in several ways. First of all, we will vary C_s so as to mimic a journey from a continental area to the coastline; that is, in the expression $C_s = \rho c_p h_s$, we will vary h_s from 10 cm to several meters. In the interior of a continent, we equate the thermal interia of the soil to that of a thin layer of water (10 cm), while at the coast line the ocean's mixed layer ($\approx$10 m) seems to be relevant. In Fig. 13 the day-to-day correlation [$\rho_1{}^c(1)$], the month-to-month correlation [$\rho_{30}{}^c(30)$] and the variance of $\hat{T}_a$ are plotted as a function of h_s, that is, the thermal inertia of the underlying boundary. In these experiments all other factors are kept constant; that is, $\alpha = 30$ J m^{-2} K^{-1} s^{-1}, $\beta = 15$ J m^{-2} K^{-1} s^{-1}, and $C_a = (\rho c_p 200) = 240\,000$ J m^{-2} K^{-1}. Also the $\hat{T}_f$ forcing numbers are the same for different h_s. The results are at least instructive. With increasing h_s ($0.5 < h_s < 7$ m), $\rho_{30}{}^c(30)$ increases while $\rho_1{}^c(1)$ is slowly decreasing. If we call $h_s = 1$, Denver and $h_s = 7$, San Diego or New Orleans we see, just as in the real world's observations, that the geographical variation of $\rho_1{}^c(1)$ does not predict how $\rho_{30}{}^c(30)$ will vary. Contrary to popular belief, we also notice that increasing interaction with the lower boundary makes the variance of $\hat{T}_a$ decrease. Similarly the variance of 30-day mean $\hat{T}_a$ (not shown) decreases monotonically from 2.42°C^2 at $h_s = 0.1$ m to 1.60°C^2 at $h_s = 7$ m.

The asterisks on the extreme left and right give the limiting values of $\rho_1{}^c(1)$, $\rho_{30}{}^c(30)$ and var($\hat{T}_a$) for $C_s = 0$ (left) and $C_s = \infty$ (right). It is surprising that autocorrelation (for any lag and any time average) is identical in the middle of the idealized continent ($C_s = 0$) and the middle of the idealized ocean ($C_s = \infty$). However, for $C_s = 0$, (12) and (13) reduce to

$$C_a \frac{d\hat{T}_a}{dt} = -\alpha(\hat{T}_a - \hat{T}_f),$$

whereas for $C_s = \infty$, $\hat{T}_s = 0$ and (12) and (13) become

$$C_a \frac{d\hat{T}_a}{dt} = -(\alpha + \beta)\hat{T}_a + \alpha\hat{T}_f.$$

In both cases, the spectrum of $\hat{T}_a$ virtually is identical to that of $\hat{T}_f$ [and hence $\rho_1{}^c(1) = 0.61$ and $\rho_{30}{}^c(30) = 0.03$]; this is because of our choice of α, β and C_a. The only difference is that the total variance of $\hat{T}_a$ is

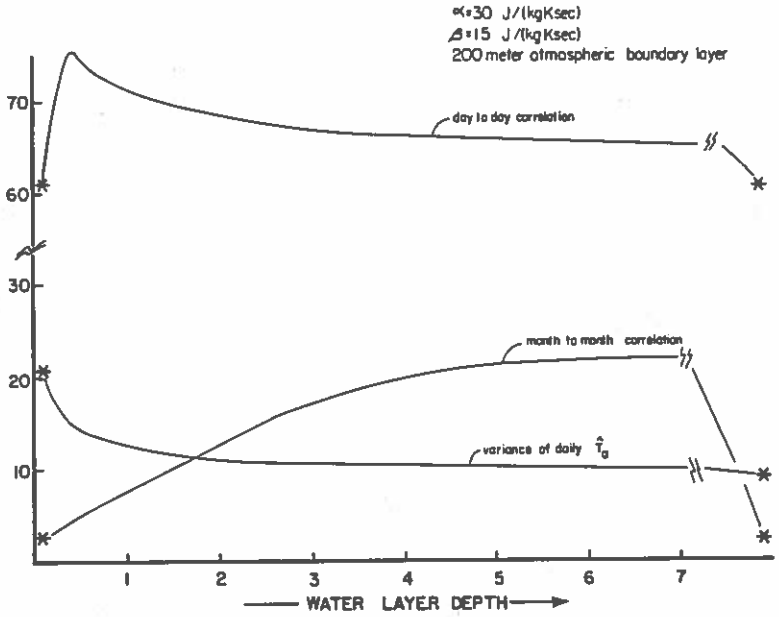

FIG. 13. Day-to-day correlation (%), variance of daily air temperature (°C^2) and month-to-month correlation (%) in an intuitive model of air–sea (or land) interaction as a function of the depth of surface water layer.

smaller in the $C_s = \infty$ case because the damping is so much larger. The location of the maximum in the $\rho_1^c(1)$ and $\rho_{30}^c(30)$ curves in Fig. 13 expresses the shallowness of the layer of water as perceived by high $[\rho_1^c(1)]$ and low $[\rho_{30}^c(30)]$ frequencies. Three meters of water is deep for high frequencies (that is $\hat{T}_s$ does not change much due to high frequency forcing), whereas the same water depth is fairly shallow at low frequencies.

Our intuitive model, (12) and (13), gives a qualitative explanation of high month-to-month persistence in the presence of interaction with the lower boundary. In fact, (12) and (13) are the differential equation analogue of a second order autoregressive process. In terms of departure from a first order process, the reason for high month-to-month persistence in the model, as well as at all 12 stations studied in section 5, is that $\rho_1^c(k)$ exceeds $[\rho_1^c(1)]^k$ for all lags longer than a few days.

From the series of monthly mean $\hat{T}_f$ and $\hat{T}_a$, we constructed a specified $\hat{T}_a$ using simultaneous $\hat{T}_f$ as the specifier. Similar to section 6, we then decomposed $\hat{T}_a = \hat{T}_c + \hat{T}_r$, a circulation specified monthly anomaly plus a residual. For low (high) values of h_s, month-to-month persistence in $\hat{T}_a$ is entirely due to the lagged product $\hat{T}_c\hat{T}_c(\hat{T}_c\hat{T}_r)$, while $\hat{T}_r\hat{T}_c$ and $\hat{T}_r\hat{T}_r$ remain small. The importance of the $\hat{T}_c\hat{T}_r$ term in areas where persistence is high agrees favorably with the conclusions arrived at in section 6.

The model based on (12) and (13) allows us some obvious extensions. (i) If we vary the spectrum of $\hat{T}_f$ (while keeping α, β, C_a and C_s constant), so as to mimic seasonality of the spectrum of free atmospheric forcing, the spectrum of $\hat{T}_a$ will vary correspondingly. (ii) The geographical distribution of persistence can be further modified by an extra term $(\gamma\hat{T}_s)$ in the right-hand side of (13), mimicking a linear feedback of temperature on albedo. The effect of this feedback is to increase the lifetime of $\hat{T}_s$ and indirectly $\hat{T}_a$. (iii) In (12) and (13), T_s anomalies were all forced by the atmosphere. The extreme persistence along California's coast (0.45) can be explained only by including another forcing in (13), with long time scales, which could represent the autonomous role of the ocean in creating T_s anomalies, and indirectly a $\hat{T}_r\hat{T}_r$ term.

Finally, it would be a nontrivial exercise to design an intuitive model that explains the maximum in persistence in summer. Since Fig. 5 indicates that this maximum is geographically restricted to the north central states, and since Fig. 12 rules out that the circulation aloft is the dominant cause of summer persistence, we have to create an intuitive model in which local factors create long-lived anomalies. In this area (and in summer), we can only think of soil moisture as being that local factor. An intuitive model would have to include feedbacks between surface temperature and evaporation, while the forcing includes rainfall anomalies in addition to $\hat{T}_f$ anomalies. Since such a model is nonlinear, it is not possible to maintain the simplicity of (12) and (13) so we postpone this task to a future date.

8. Summary

In this paper we have addressed the persistence of monthly surface air temperature in terms of several factors which contribute to it. These factors include the persistence of day-to-day weather fluctuations, the variability of the large-scale (700 mb) circulation on the monthly time scale, and small-scale effects involving surface boundary anomalies. The following is a summary of the major findings and implications.

The month-to-month persistence over the United States is characterized by low values in the continental interior and by relatively high values in coastal regions, especially along the West Coast. The main exception to this pattern is the persistence maximum which occurs in the north central states during the summer season. The corresponding autocorrelations of the anomaly patterns show a maximum in winter and a secondary maximum in summer. Detrending reduces the autocorrelations in all months, although the pattern correlations at lags 2 and 3 months for even the detrended data are much larger than would be expected from a first-order Markov process. The reduction of persistence by detrending is greatest in summer. The portion of the persistence attributable to low-frequency variability is therefore largest in summer.

Because the day-to-day persistence of surface air temperature anomalies was found to be quite similar ($\approx$0.70) in vastly different climatic regions of the United States, the geographical variations of month-to-month persistence cannot be attributed to the geographical variation of the day-to-day persistence. At nearly all the stations studied here, the presence of nearby bodies of water seems to determine whether the month-to-month persistence exceeds that to be expected from the day-to-day persistence. This conclusion is consistent with the results derived from an intuitive energy balance model in which the soil (or ocean) surface layers and the atmospheric boundary layer respond to daily fluctuations in the free atmosphere. The results obtained here also support the findings of Madden and Shea (1978) insofar as the difference between monthly- and daily-derived persistence is a measure of potential predictability. Month-to-month persistence has the advantage that it can be easily implemented in an operational setting.

The (700 mb) circulation-derived temperature specifications provide an informative framework for the decomposition of monthly temperature persistence. Of the four products involving the concurrent and lagged values of the circulation-derived $(\hat{T}_c)$ and residual $(\hat{T}_r)$ portions of the monthly mean temperature anomalies, the terms $\hat{T}_c\hat{T}_c$ and $\hat{T}_c\hat{T}_r$ account for most of the winter maximum of persistence. Whereas $\hat{T}_c\hat{T}_c$ represents that portion of the temperature persistence attributable to the persistence of the 700 mb circulation, $\hat{T}_c\hat{T}_r$ represents the temperature persistence unexplained by the concurrent circulation but correlated with the circulation anomalies of the *antecedent* month. The fact

that $\hat{T}_c\hat{T}_r$ exceeds $\hat{T}_c\hat{T}_c$ in most months and most areas is intriguing, as it implies that SST and/or land surface anomalies induced by the *antecedent* circulation are responsible for a greater portion of the surface temperature persistence than is the concurrent circulation. This finding is indicative of a feedback of circulation-induced SST anomalies onto subsequent monthly air temperatures in the atmospheric boundary layer in coastal regions. Similar feedback by snow cover and soil moisture anomalies may also be indicated, since the distributions of the latter variables are dependent on antecedent circulation patterns. Because $\hat{T}_c\hat{T}_r$ consistently exceeds $\hat{T}_c\hat{T}_c$ during the summer months when the persistence over the continental interior reaches its maximum, a role of soil moisture at interior stations is suggested.

The surface-to-700 mb feedback term $\hat{T}_r\hat{T}_c$ is the smallest of the four terms considered in the specification framework. This term is consistently positive in the late spring and summer months for which Namias's (1980) proposed mechanism of drought maintenance should be most effective. However, since the values of $\hat{T}_r\hat{T}_c$ never exceed 0.05, they cannot be convincingly distinguished from sampling errors.

Finally, the major portion of the abrupt decay of monthly temperature persistence with inland distance is determined by $\hat{T}_r\hat{T}_r$, which represents the contribution of the persistence of temperature anomalies attributable to local effects (e.g., advection of SST anomalies). The fact that $\hat{T}_r\hat{T}_r$ is much larger along the California coast than along the Gulf of Mexico or Atlantic coasts implies that either a) SST anomalies are less persistent along the Gulf and East Coasts or b) advection from the ocean is stronger in California than along the Gulf and East Coasts. Because $\hat{T}_r\hat{T}_r$ is largest along the West Coast and smallest along the East Coast in a zone of predominantly west-to-east airflow, the frequency of advective events is likely an important contributor to $\hat{T}_r\hat{T}_r$.

Acknowledgments. The research was supported by the Climate Dynamics Program, Division of Atmospheric Sciences, National Science Foundation, under Grants ATM-8314431 and ATM-8313726 and by the Department of Energy under Contract DE-AS05-81EV-10539. We are grateful for technical assistance received from Robert Kaylor, Hal Bloom and Chuck Mulchi, and the Computer Science Center at the University of Maryland.

REFERENCES

Cayan, D. R., and A. V. Douglas, 1984: Urban influences on surface temperatures in the southwestern United States during recent decades. *J. Climate Appl. Meteor.*, **23**, 1520–1530.

Dickson, R. R., 1967: The climatological relationship between temperatures of successive months in the United States. *J. Appl. Meteor.*, **6**, 31–38.

Gutzler, D. S., and K. C. Mo, 1983: Autocorrelation of Northern Hemisphere geopotential heights. *Mon. Wea. Rev.*, **111**, 155–164.

Horel, J., 1985: Persistence of the 500-mb height field during Northern Hemisphere winter. *Mon. Wea. Rev.*, **113**, 2030–2042.

Karl, T. R., 1985: Intraseasonal variability of extremely cold and warm months in the contiguous United States. *J. Climate Appl. Meteor.*, **24**, 215–227.

Klein, W. H., 1983: Objective specification of monthly mean surface temperature from mean 700-mb height in winter. *Mon. Wea. Rev.*, **111**, 674–691.

——, 1985a: Specification of monthly mean anomalies of surface air temperature in Canada and Alaska. *Atmosphere–Ocean*, **23**, No. 2.

——, 1985b: Space and time variations in specifying monthly mean surface temperature from the 700 mb height field. *Mon. Wea. Rev.*, **113**, 277–290.

Madden, R. A., 1977: Estimates of autocorrelations and spectra of seasonal mean temperatures over North America. *Mon. Wea. Rev.*, **105**, 9–18.

——, and D. J. Shea, 1978: Estimates of natural variability of time-averaged temperatures over the United States. *Mon. Wea. Rev.*, **106**, 1695–1703.

Munk, W. H., 1960: Smoothing and persistence. *J. Meteor.*, **17**, 92–93.

Namias, J., 1952: The annual course of month-to-month persistence in climatic anomalies. *Bull. Amer. Meteor. Soc.*, **33**, 279–285.

——, 1953: Thirty-day forecasting: a review of a ten-year experiment. *Meteor. Monographs*, Amer. Meteor. Soc., **2**, No. 6, p. 83.

——, 1959: Persistence of mid-troposphere circulations between adjacent months and seasons. *Rossby Memorial Volume*, Rockefeller Institute Press and Oxford University Press, 240–248.

——, 1978: Persistence of U.S. seasonal temperatures up to one year. *Mon. Wea. Rev.*, **106**, 1157–1167.

——, 1980: Severe drought and recent history. *J. Interdisciplinary History*, X:4, 697–712.

Roads, J. O., and T. P. Barnett, 1984: Forecasts of the 500-mb height using a dynamically oriented statistical method. *Mon. Wea. Rev.*, **112**, 1354–1369.

Straus, D. M., and M. Halem, 1981: A stochastic-dynamical approach to the study of the natural variability of the climate. *Mon. Wea. Rev.*, **109**, 407–421.

Trenberth, K. E., 1985: Autocorrelations of daily geopotential height over the Southern Hemisphere. *Mon. Wea. Rev.*, **113**, 38–53.

van den Dool, H. M., 1984: Long-lived air temperature anomalies in the midlatitudes forced by the surface. *Mon. Wea. Rev.*, **112**, 555–562.

——, and J. L. Nap, 1981: An explanation of persistence in monthly mean temperatures in the Netherlands. *Tellus*, **33**, 123–131.

——, and R. E. Livezey, 1984: Geographical distribution and seasonality of month-to-month correlation of monthly mean 700-mb heights. *Mon. Wea. Rev.*, **112**, 610–615.

van Loon, H., and R. L. Jenne, 1975: Estimates of seasonal mean temperatures, using persistence between seasons. *Mon. Wea. Rev.*, **103**, 1121–1128.

Walsh, J. E., 1984: Forecasts of monthly 700 mb height: Verification and specification experiments. *Mon. Wea. Rev.*, **112**, 2135–2147.

——, and A. Mostek, 1980: A quantitative analysis of meteorological anomaly patterns over the United States, 1900–1977. *Mon. Wea. Rev.*, **108**, 615–630.

——, W. H. Jasperson and B. Ross, 1985: Influences of snow cover and soil moisture on monthly air temperatures. *Mon. Wea. Rev.*, **113**, 756–768.